

PROCEEDINGS OF SPIE

[SPIDigitalLibrary.org/conference-proceedings-of-spie](https://spiedigitallibrary.org/conference-proceedings-of-spie)

Lasers with intra-cavity phase elements

A. Alkan Gulses, Russell Kurtz, Gabriel Islas, Igor Anisimov

©2015 SPIE. One copy may be downloaded for personal use only.

A. Alkan Gulses, Russell Kurtz, Gabriel Islas, Igor Anisimov, "Lasers with intra-cavity phase elements," Proc. SPIE 10513, Components and Packaging for Laser Systems IV, 1051318 (20 February 2018); doi: 10.1117/12.2291829

SPIE.

Event: SPIE LASE, 2018, San Francisco, California, United States

Lasers with Intra-Cavity Phase Elements

A. Alkan Gulses, Russell Kurtz, Gabriel Islas
Luminit, LLC, Torrance, CA 90501

Igor Anisimov
Air Force Research Laboratory, Wright-Patterson AFB, OH 45433

ABSTRACT

Conventional laser resonators yield multimodal output, especially at high powers and short cavity lengths. Since high-order modes exhibit large divergence, it is desirable to suppress them to improve laser quality. Traditionally, such modal discriminations can be achieved by simple apertures that provide absorptive loss for large diameter modes, while allowing the lower orders, such as the fundamental Gaussian, to pass through. However, modal discrimination may not be sufficient for short-cavity lasers, resulting in multimodal operation as well as power loss and overheating in the absorptive part of the aperture.

In research to improve laser mode control with minimal energy loss, systematic experiments have been executed using phase-only elements. These were composed of an intra-cavity step function and a diffractive out-coupler made of a computer-generated hologram. The platform was a 15-cm long solid-state laser that employs a neodymium-doped yttrium orthovanadate crystal rod, producing 1064 nm multimodal laser output. The intra-cavity phase elements (PEs) were shown to be highly effective in obtaining beams with reduced M-squared values and increased output powers, yielding improved values of radiance. The utilization of more sophisticated diffractive elements is promising for more difficult laser systems.

Keywords: laser cavities, diode-pumped solid-state laser, DPSS, laser beam quality, diffractive phase elements, diffractive optical elements, computer-generated hologram, CGH

1. INTRODUCTION

As the importance of lasers rises in almost every principal field of technology, such as defense, telecom, micromachining, and medical as a few examples, control of intensity distribution has gained much more interest, resulting in many new directions that enrich the area of laser science [1].

Transverse field distribution of a laser determines the beam's divergence angle, making it an extremely important factor in characterizing the beam's performance, such as focusability or long-range (over a km) propagation. The distribution is characterized by transverse modes, each of which corresponds to a solution of the wave equation in a cavity. Solutions can be successfully estimated by solving the wave equation subject to any cavity geometry and by assuming that amplitude of the wave changes much slower in the propagation direction than transverse directions [2].

In controlling laser intensity, obtaining both high optical power and good beam quality simultaneously has always been a difficult task. Elongated resonator geometries help in the case of gas or solid-state laser systems; the small features of semiconductor lasers, however, put stringent limits on their output beams. To overcome those limits and to use the benefits of the so-called vertical cavity surface emitting lasers (VCSELs), vertical external cavity surface emitting lasers (VECSELs) were introduced recently [3]. In that scheme, the curved out-coupler mirror is separated from the semiconductor laser cavity, resulting in beams with better quality. Despite their superiority in quality, VECSELs have certain drawbacks and limits caused mainly by their elongated cavity, requiring extra space and, potentially, inducing instability. Therefore, a need for passive elements to improve laser beam quality is emergent to improve performance in a compact manner.

Transmissive phase elements (PEs) or phase masks are diffractive optical elements (DOEs) that can shape the coherent light with minimal loss. While they can be as simple as gratings or step functions, sophisticated DOEs, such as computer-generated holograms (CGHs), can execute more complicated tasks [4]. A CGH works by selectively

diffracting light through its digitally designed pixels. Thereby, it modulates wavefronts in a desired way. In general, CGHs are used in miscellaneous applications in 2D/3D imaging, aberration correction, fiber-optic interconnects and beam shaping. Laser beam shaping can be executed in two different ways: internal and external. The former has obvious advantages over the latter. The intra-cavity mode shaping scheme modulates the laser in its forming stage so that more fundamental improvements can be done using the entire optical power and volume. This means that one can create modes with large sizes encircling higher powers as well as eliminating higher-order modes. If this elimination is made with traditional opaque aperture windows by absorption, for example, energy loss and extra heating occur, reducing overall quality. If, on the other hand, when a transmissive phase mask is used, power loss can be minimized with even improved functionality through clever design of the mask, i.e., by using advanced formats possessed by CGHs. Therefore, in principle, it is possible to select, control, and modify the modes of a high-power laser with a CGH, and even to compensate for a short cavity length. In fact, some works in the literature, mostly theoretical, discuss modal selectivity of intra-cavity elements [5-8].

In this research, we first studied the design of intra-cavity diffractive elements, which can also be used as out-coupling mirrors. We then worked on the systematic experiments on a variety of intra-cavity diffractive PEs. These results are compared to that of a simple opaque aperture window instead of any PE. The comparison helps us to find properties of intra-cavity PEs for lasers in general, and to determine the types of cavity in which intra-cavity PEs are superior. Our main experimental platform was an open cavity diode-pumped solid-state (DPSS) laser on an optical breadboard. DPSS lasers typically have high round-trip gain, enabling operation even with lossy intra-cavity elements (such as the opaque aperture). Also, the open cavity structure made it easy to modify the laser. In the organization of this paper, we describe laser cavity mathematics, application of matrix mechanics to simulations, and the design of intra-cavity PEs in Section 2. Certain figures of quality are explained in Section 3, followed by demonstration of comprehensive experimental data. Section 4 continues with possible applications and conceptual futuristic designs, which will harness the power of compatibility of laser light and diffractive optics in general. This section also describes our future work and its possible evolution. The paper is summarized and concluded in Section 5.

2. THEORY OF INTRA-CAVITY PHASE ELEMENTS

2.1 Laser Cavity Matrix Mechanics

Amplified by the active medium, light propagates back-and-forth in a resonator between mirrors, yielding different modes of electromagnetic (EM) radiation. A mode can simply be defined as an EM configuration that maintains its form after one round-trip. So, an eigenvalue equation with a round-trip propagation operator \hat{P} can be used to define cavity dynamics, given as [9],

$$\hat{P}\Psi_{mn} = \gamma_{mn}\Psi_{mn} \quad (1)$$

where Ψ_{mn} represents an eigenvector defining spatial distribution of the mode and γ_{mn} denotes an eigenvalue that relates that specific mode to its power, indicating its dominance in the cavity. An analytical solution of Equation (1) requires diagonalization of the propagation matrix \hat{P} , which is inconvenient most of the time, and becomes untenable in analyzing complicated systems. Instead, the mode propagation within the cavity can be simulated through iterations along the light path by the Fox-Li method [10]. Numerical results obtained by this method can be quite convenient, accurate, and computationally fast. Furthermore, different intra-cavity elements can be expressed mathematically with appropriate matrices, enabling rapid tests of many different configurations.

In a DPSS laser with total length L , such as the one shown in Figure 1(a), the laser crystal, optical pump, and mirrors define the cavity. Mirrors are at a planar-concave configuration, where the concave mirror introduces refractive power. Apertures in the system are created by the pump spot and the crystal's physical thickness, denoted as t . The crystal's length is shown as l . Mirror 1 is a planar mirror transparent to the pump wavelength. The distances between Mirror 1 and the crystal is z_1 , from the crystal to the PE is z_2 , and from the PE to the (curved) output coupler is z_3 . The PE may be placed anywhere in the cavity; it diffracts the beam so as to shape the available modes.

In a more advanced scheme, depicted in Figure 1(b), the PE, integrated with a planar out-coupler in a plane-parallel (two planar mirrors constitute the resonator) cavity configuration, shapes the modes by also including the effect of the curved mirror.

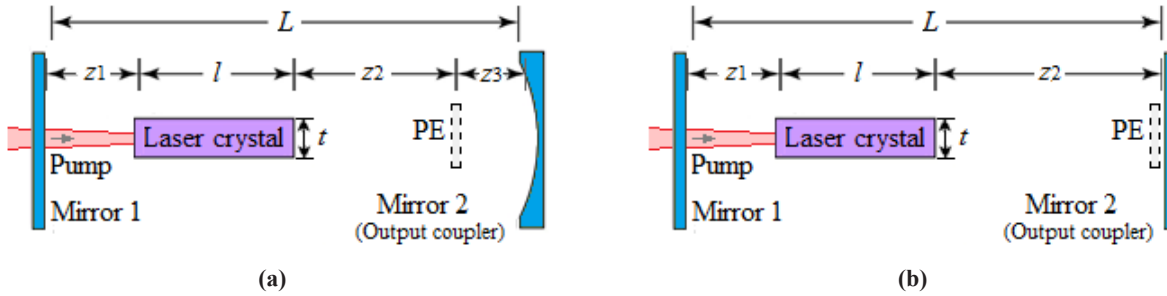


Figure 1. Common DPSS laser configurations to demonstrate novel diffractive PEs, comprising (a) a planar-concave cavity having a PE and (b) a plane-parallel cavity with a PE attached at the output coupler. L , z_1 , z_2 , z_3 , l , and t are defined as specific parameters.

These two configurations demonstrate the main schemes in applying diffractive intra-cavity elements to lasers. For the one shown in Figure 1(b), where the element is combined with the mirror, the term “graded phase mirror” might be used as well [9]. That modeling removes the necessity of a curved mirror, and thus introduces more control, accuracy, and larger spot sizes for the output.

As an evaluation tool, every available element is expressed as an operator listed in Table 1. Iterative motion of the EM field in the cavity can be considered as a serial propagation along a sequence of lenses [2]. Therefore, a concave mirror with radius of curvature R is shown by a lens profile function in the first row, where \hat{M} is the mirror operator, with positive dioptric power. The aperture operator, \hat{A} , can be any plane geometric shape, such as rectangular or elliptical. Square and circle forms are special cases of these two, shown in Table 1. \hat{A} takes a and b as inputs for spatial extensions in x and y , and applies conditions to compute functions called *rect* and *ell*. In the last row, the propagation operator \hat{H} is the spatial translation function operator coming from the Huygens-Fresnel principle [11], for a distance z . The parameters f_x and f_y are defined as spatial frequencies along x and y . The propagation operator is different from the others in that, while the other operators are applied in the spatial domain, \hat{H} operates in the frequency domain. To execute, one needs to take a Fourier transform of the wave field defined by a spatial extent ($T \times T$), apply the operator, and then take an inverse transform to return to the spatial coordinates. The parameter T defines the total feature size of the simulation area ($x_{\max} = y_{\max} = T/2$, assuming that the origin is at the center). The conditions in the right-most column for \hat{M} and \hat{H} come from the Shannon-Nyquist sampling theorem [12], where δ is the sampling interval ($\delta_x = \delta_y \equiv \delta$, for simplicity). Therefore, sampling limits the maximum spatial extent of the simulation area, minimum feature size, radius of curvature of the mirror, and propagation distance. The distance restriction condition seen at the bottom row for propagation, is not very restrictive given the nominal cavity parameters. For longer propagation distances, for example in atmospheric propagation research, different and more approximate techniques can be used [13].

Table 1. Common operators for analytical evaluation of cavities. Variables: x, y are transverse coordinates with corresponding spatial frequencies f_x, f_y , and z is the longitudinal coordinate. Parameters: a, b are lateral dimensions, R is radius of curvature, δ and T are sampling grid size and total lateral size. Finally, λ is the wavelength of the laser emission. See text for more explanations.

Function	Operator	Condition
Concave mirror (lens function)	$\hat{M} = \exp \left[-i \frac{2\pi}{\lambda R} (x^2 + y^2) \right]$	$R \geq \frac{2\delta T}{\lambda}$
Rectangular aperture	$\hat{A}_r = \text{rect} \left(\frac{x}{a} \right) \text{rect} \left(\frac{y}{b} \right)$	$ x \leq \frac{a}{2}, y \leq \frac{b}{2}$
Elliptical aperture	$\hat{A}_e = \text{ell} \left(\frac{x}{a}, \frac{y}{b} \right)$	$\frac{x^2}{a^2} + \frac{y^2}{b^2} \leq 1$
Propagation (for distance ‘ z ’)	$\hat{H} = \exp \left[i2\pi z \sqrt{\frac{1}{\lambda^2} - (f_x^2 + f_y^2)} \right]$	$z \leq \frac{\delta T}{\lambda}, \quad \frac{-1}{2\delta} \leq f_{x,y} < \frac{1}{2\delta}$

In determining the round-trip propagation operator \hat{P} , these operators are applied in a proper sequence. For example, in Figure 1(a) without any element, one round-trip starts with the pump laser reaching the crystal. Furthermore, when computing \hat{P} , the sequence of operators starts from the right so that, $\hat{P} = \hat{H}_{2z_1} (\hat{A}_r \hat{H}_l \hat{A}_r) \hat{H}_{2z_2} \hat{M} \hat{H}_{z_2} (\hat{A}_r \hat{H}_l \hat{A}_r)$. Here, from

right to left, \hat{A}_r is the square aperture of the crystal defined in Table 1, where $a = b = t$ for the rectangular aperture. An elliptical pump spot aperture, \hat{A}_e , can be taken instead of \hat{A}_r since it determines the lasing area, particularly if this is much smaller than the crystal cross-section. This is followed by propagation in the crystal, \hat{H}_l . Normally, the crystal may be birefringent and have different refractive indices for x and y (transverse) axes. That can be represented by modulating \hat{H} from Table 1, by first representing it in Fresnel approximation format and separating x and y sections, and then using different wavelengths accordingly. An easier way, however, is to represent that by using ellipticity of the pump spot, which will be explained later. Thus, after leaving the crystal's aperture, the beam propagates a distance z_2 , shown by \hat{H}_{z_2} . The next element on the path is the concave mirror, \hat{M} , followed by propagation back to the crystal. Then, the beam passes through the crystal again (note that, in the expression, the crystal operators are shown in parenthesis: $(\hat{A}_r \hat{H}_l \hat{A}_r)$). The leftmost operator is \hat{H}_{2z_1} , expressing propagation along z_1 , left and right sequentially (two times the distance z_1), since the planar mirror has no effect.

Therefore, in the application of a cavity simulation, the initial field Ψ can be chosen as unity in the beginning, and iterations upon repetitive application of the round-trip operator, \hat{P} , shapes Ψ , which is defined by the modal indices m and n , until final modal distribution Ψ_{mn} settles down. Having defined the basic tools of analysis, miscellaneous DOEs, including both simple and complex intra-cavity PEs, can be designed and analyzed through those methods.

2.2 Design of Phase Elements

Diffractive PEs can effectively transform one wavefront to another. Intra-cavity PEs (one or more) can be used in a cavity with optical power (provided by one or more concave mirrors or intra-cavity lenses) or with no optical power (a plane-parallel configuration supplied by two planar mirrors). We will examine these two main scenarios with comparisons below. In the PE design, the thin element approximation (TEA) will be used where the physical thickness of the element may reasonably be neglected for functionality. We ignore material absorption in the PEs, so all the EM power is diffracted and redirected onto the desired path, permitting absorption by the apertures in the system.

The PEs that are examined below are a phase-step function and a more complex computer-generated hologram. Furthermore, an opaque aperture is analyzed for comparison. These elements are sketched in Figure 2 and expressed analytically in Table 2.

(a) PE1: Phase-Step Function (PSF)

A straightforward way to develop a diffractive correction to a system is to express the mathematical function of the element under consideration. If the system pictured in Figure 1(a) is considered, as the laser field builds inside, a PE can be used to select a mode, or a set of modes, enhanced afterwards. For such a system, where refractive power is supplied by the mirror, it is possible to use a simple approach both for design and fabrication in practical applications. The three main PEs that we have examined are sinusoidal grating, square grating, and step function. Based on our analysis, step function is effective in obtaining an almost pure Gaussian beam, and it is easier to fabricate. This PSF has a profile given in Figure 2(b) and in Table 2, second row. Its size, defined by α , is chosen based on the expected Gaussian spot size for the cavity under consideration. Its step height, defined by β , is chosen to induce a phase shift of π , resulting in controlled interference of modes outside the step area. Its location, defined by z_3 , has also been investigated, and was shown to have minimal results on the output. Therefore, the PSF will implicitly amplify the Gaussian via its surface, by also providing redirection of other modes with little absorptive loss. To observe the effects and to optimize the size of the PSF, the operator $\hat{P}\hat{S}\hat{F}$ can be placed appropriately in the operator sequence of the cavity by adjusting the lengths. The resulting Ψ_{mn} can then be found, together with its associated γ_{mn} .

(b) PE2: Computer-Generated Hologram (CGH)

CGHs are DOEs that have computationally designed diffractive structures [4]. They can provide phase or amplitude modulation and their profiles do not necessarily show a periodic pattern (like a grating). Phase-only CGHs are effective in executing complex functions since they are not absorptive and do not have large space-bandwidth-product requirements (like non-phase-only CGHs). Thus, the phase relief structure of any CGH can itself be defined as a function of kind $f(x, y)$, as shown in Figure 2(c) and in Table 2, third row.

Upon designing an intra-cavity CGH, one needs to start with a desired pattern, let's say a Gaussian of the form $\Psi_{00}(x, y)$ at one end of the cavity in Figure 1(b). Then, one cavity pass for length L , from left to right, is calculated as: $\hat{C}_L = \hat{H}_{z_2} (\hat{A}_r \hat{H}_l \hat{A}_r) \hat{H}_{z_1}$, where \hat{C}_L is one pass operator, and applied onto the desired output. Then the CGH function $f(x, y)$ is found at the out-coupler mirror as [14, 15],

$$C\hat{G}H = f(x, y) = \frac{(\hat{C}_L \Psi_{00})^*}{\hat{C}_L \Psi_{00}} \quad (2)$$

Therefore, in Equation (2), one resonator pass is complex-conjugated and divided by itself. The derivation follows the fact that when $C\hat{G}H$ is expressed as in Equation 2, one round-trip yields itself. Therefore, if one starts with a desired pattern, and computes the CGH followed by placing the element in the cavity amongst other cavity operators as explained before (this time no mirror operator), the system will stagnate at the state of the desired pattern, after enough iterations. The desired form can be anything containing allowed modes, such as TEM_{00} , TEM_{10} , or a combination of these modes. The size of the mode also depends on the design. Unlike the PSF, which selects a mode out of existing ones, the CGH-assisted cavity will create its own modal patterns. We assign a relatively large Gaussian as an input, stated as $\Psi_{00} = TEM_{00}$.

Fabrication of diffractive elements is an important issue as precision makes a large difference in their operation. The minimum step height (β) plays an important role in CGH effectiveness. The physical phase depths of a CGH profile can be calculated by using Equation (3),

$$\beta_{CGH} = \frac{\lambda}{Q \Delta n} \quad (3)$$

where Q is the number of phase quantization levels and Δn is the refractive index difference between air and the CGH material. There will be 2π phase difference between the deepest and the highest pixels on the CGH. Therefore, as one can get the phase profile from Equation (2), step height definition is found from Equation (3). These are the necessary tools to determine the entire pattern for fabrication.

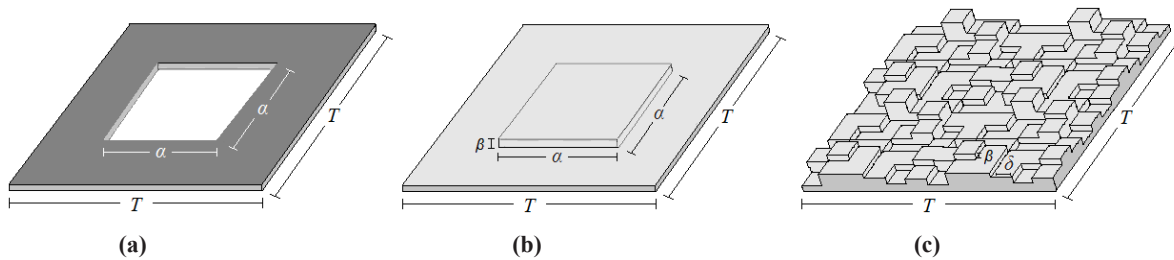


Figure 2. Sketches of (a) an opaque aperture (OPA) of feature size α , (b) a transparent PSF of size α and depth β , (c) conceptual representation of a transparent phase-only CGH with pixel size equal to its sampling size of δ and minimum phase depth β .

Table 2. PEs used in laser cavity are summarized. PSF has a relief height β , and window size $\alpha \times \alpha$. The PSF is zero outside the interval stated in the Condition column. CGH has a format that is calculated computationally, and its area cannot exceed the available area, as stated in the Condition column. Here, (x, y) shows the plane of interest.

Function	Operator	Condition
Opaque Aperture	$\hat{A}_r = \text{rect}\left(\frac{x}{\alpha}\right) \text{rect}\left(\frac{y}{\alpha}\right)$	$ x \leq \frac{\alpha}{2}, y \leq \frac{\alpha}{2}$
PE1: Phase-step function (PSF)	$P\hat{S}F = \exp\left[i \frac{2\pi n}{\lambda} \beta\right]$	$ x \leq \frac{\alpha}{2}, y \leq \frac{\alpha}{2}$
PE2: Computer-generated hologram (CGH)	$C\hat{G}H = f(x, y)$	$ x \leq \frac{T}{2}, y \leq \frac{T}{2}$

3. EXPERIMENTAL DEMONSTRATION OF INTRA-CAVITY PHASE ELEMENTS

3.1 Parameters of Evaluation

In expressing the beam divergence, one of the important parameters is M^2 formalism, the beam propagation ratio, defined as the product of the beam waist radius and divergence angle of the beam. A perfect Gaussian beam defines

$M^2 = 1$, as reference. For high-energy multimode lasers, that value may increase up to 30 or 40. The M^2 factor is important in characterizing the quality since it describes the propagation characteristics (spreading rate) of laser beams. In general, the smaller the M^2 value, the better quality a beam has.

Another factor while analyzing the quality of a laser beam is the figure of merit (FOM), where the beam power is also taken into account. The beam's quality factor, FOM, is essentially the radiance (or brightness), and is defined as output beam power divided by the square of the M^2 . For an ideal laser under consideration, output power increases with input power. Since M^2 also increases with output power (the higher the power, the greater the number of modes supported), FOM can be expected to be almost constant with respect to power variations for a laser system. That gives a relatively efficient platform for beam quality evaluation for certain modifications.

3.2 Experiments

Experiments have been executed by considering the two main configurations as given in Figure 1. The platform was a neodymium doped yttrium orthovanadate (Nd:YVO₄) rectangular crystal rod of aperture (t) equal to 4 mm, and length (l) equal to 30 mm. Cavity length (L) is 150 mm. And, z_1 is 20 mm. Total of z_2 and z_3 is 100 mm. In the experiments, z_3 was estimated as 3 millimeters. The reflectivity of each mirror is 0.998, and the radius of curvature of the concave mirror is 1000 mm.

The pump power at 808 nm was limited to just over 8 W, and the pump was operated at a 20% duty cycle with a repetition rate of 150 Hz. The pump emission, provided by a diode laser, was coupled into the cavity by a lens focused into the crystal from the left through the planar mirror. In terms of technical operability, the 808 nm pump laser was controlled by a Thorlabs (LDC4020) laser diode controller. The current was adjustable from 0-20 A with a compliance voltage of 11 V. The cooling was accomplished by mounting the laser diode to a thermoelectric (TEC) plate cooler, operated by a temperature controller, which was powered by a 12 V – 8.4 A power supply. The pump laser output was transmitted via a multimode fiber to the collimator lens, followed by a focusing lens into the cavity.

Figure 3 shows the optical workbench on which the base experiment was built. From left to right, the components are the pump laser (transported via fiber), a 120 mm focal length lens, a planar mirror, the laser crystal's aluminum cage, a stage (to place intra-cavity elements), and an out-coupling mirror. When the setup in Figure 1(a) was used, this out-coupling mirror was the curved mirror. On the other hand, when Figure 1(b) was valid, the out-coupler was a CGH-attached planar mirror. This was achieved by attaching the back surface of the CGH to the planar mirror with an index matching liquid. After the out-coupling mirror, a notch transmission filter would eliminate residual pump light.

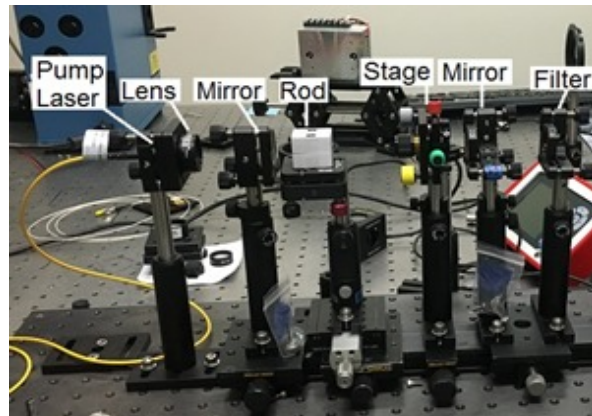


Figure 3. Experiment setup: (from left to right) pump laser, focusing lens, planar mirror, laser rod, empty stage, out-coupling mirror, and filter.

When the laser was in its base configuration, without an auxiliary diffractive element in the system, the output was a multimodal beam whose M^2 was measured to be 4.64. Several auxiliary elements were tested in the cavity systematically. These parts are bare polycarbonate (PC) substrate (SUB), an opaque aperture (OPA), phase-step function (PSF) on PC, and computer-generated hologram (CGH) on PC. In addition, a combination of SUB+OPA was tested to determine intrinsic material loss. SUB, here, means the transparent material that carries optical elements like PSF or CGH (Figure 2(b)-(c)). Initially these phase profiles (masters) were fabricated on photoresist by means of gray-scale UV

lithography or direct-beam laser-writing processes with a 405 nm laser. Then, those patterns were replicated onto a type of epoxy resin at $\sim 30 \mu\text{m}$ thickness, sitting on PC substrate of almost $250 \mu\text{m}$ thickness. Therefore, SUB denotes a composition of thin epoxy layer on PC, and when it is placed in the cavity, that means an experiment without any diffractive correction but the material that constitutes the PEs that is inserted in the cavity. The opaque aperture, or OPA, demonstrated before in Figure 2(a), was composed of polymethylmethacrylate (PMMA), covered by black-painted aluminum sheets, with a fully transparent empty window. The designs of the PSF and CGH have been explained above. For these experiments, the PSF aperture α was 1.5 mm, the CGH pixel size (sampling distance) δ was $13.6 \mu\text{m}$, CGH quantization level Q is 16, and T , the total area under consideration, was simulated as $10 \times 10 \text{ mm}$. In practice, however, it is the area that encloses the signal area, which is much smaller than that value.

Modeling the unknowns like crystal response, thermal lensing, and exact pump spot shape is critical in simulating the system. It was noted that these three items are related to each other. As a practical methodology, a bare laser cavity has a known output pattern (in this case it was almost like TEM_{10}) and by cleverly adjusting the simulation parameters, one can get equivalent results. Thus, in this case, a simulation with an elliptical pump spot with dimensions $\sim 1.5 \times 2.5 \text{ mm}$ can be chosen to yield the experimental empty cavity output. Based on the discussion in Section 2, this means that \hat{A}_c is identified, and can be used in all simulations for testing both the empty cavity and other elements.

The results of our experiments are summarized in Figure 4 as output vs. input power, with data summarized in Table 3. In the experiments, M^2 was taken at the same input power in general but not always, due to mismatch between required powers to start laser operation.

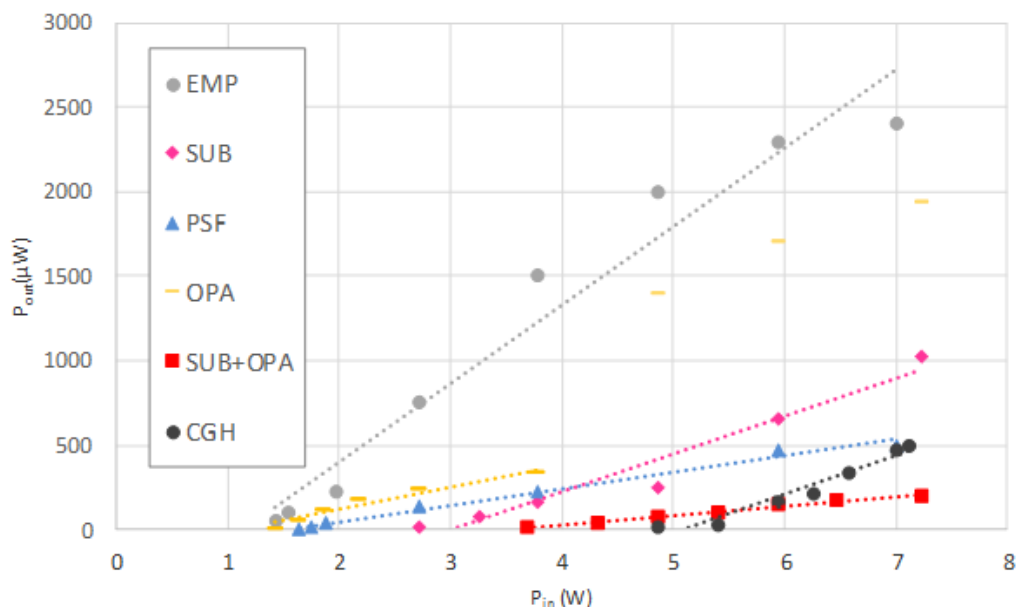


Figure 4. Input-output (slope efficiency) curves for our DPSS laser carrying a variety of passive optical elements. The x -axis is the power input (P_{in}) from the pump, and y -axis is the power output (P_{out}) from the open laser cavity. EMP = empty laser (gray circle), SUB = bare substrate material (purple diamond), PSF = phase-step function (blue triangle), OPA = opaque aperture (yellow dash), CGH = computer-generated hologram (black circle). Also, SUB + OPA is shown (red square). In linear fits, only the first portion of OPA is considered.

In Figure 4, dots represent data points and lines are linear best-fit curves. Gray color is for the empty cavity (EMP). When a piece of epoxy-covered PC without an imposed pattern is inserted, data is shown as SUB, and indicated with purple. PSF, denoting the phase element, is blue. The opaque aperture (OPA) test is shown as yellow. The combination of SUB and OPA is red, and the out-coupler CGH is black. Note that for the data in the OPA section we use the first six points (neglecting the last few). There is a large energy discontinuity for these last data points. The reason that we take the first portion of the data is because the M^2 measurement was executed closer to this input power. The reason to test SUB and OPA together is as a comparison for the optical loss supplied by the SUB (this can be minimized by both using antireflection (AR) coatings for Fresnel losses and selecting superior quality flatness optics).

Table 3. Summary of the experimental results of our modified DPSS laser. Some performance parameters are demonstrated for various intra-cavity elements. P_{th} stands for threshold power. σ_s represents slope efficiency ($P_{out} / (P_{in} - P_{th})$). M^2 and FOM are parameters under consideration (indicated by bold rectangle). See text for more information.

	EMP	SUB	OPA	SUB+OPA	PSF	CGH
P_{th} (W)	1.40	3.05	1.43	3.68	1.64	5.15
$\sigma_s (\times 10^{-4})$	5.1	2.3	1.4	0.6	1.1	2.0
M^2	4.64	3.74	3.43	2.35	2.30	1.50
FOM (μ W)	79	17	31	17	51	92
FOM' ($\times 10^{-5}$)	2.37	1.64	1.19	1.09	2.08	8.89

3.3 Discussion

We analyzed the data in Figure 4 and Table 3 together. In analyzing PE-assisted cavities, the configuration shown in Figure 1(a) was used for the simpler PSF and the scheme given in Figure 1(b) was used in demonstrating the CGH. Note that we used two FOM definitions. The usual FOM uses output power that the M^2 measurement is taken, and divided by $(M^2)^2$, whereas FOM' uses slope efficiencies instead, i.e., $FOM' = \sigma_s / (M^2)^2$, thus, a unitless quantity. We used both definitions to gain more insight and to lessen the effect of different measurement conditions caused by experimental difficulties. Results of the empty cavity experiments are reference points. When a piece of SUB was placed in the cavity to affect power, the lasing threshold P_{th} almost doubled. The M^2 seems to be lower because of power output drop (note that, most of the M^2 measurement was done at around $P_{in} \sim 4$ W, it will be mentioned when this is different) and since less power limits the number of modes. The FOM values are more reliable for evaluation and demonstrate a decrease from 79 to 17. That is also understandable since introducing this material causes intra-cavity Fresnel losses. Using AR coatings might reduce this effect. When a traditional aperture was inserted, listed in the third column as OPA, FOM increased, since now the higher order modes were filtered out. Also, P_{th} decreased to the same value as the empty cavity. To compare with PEs where a transparent material is a must, we also inserted a transparent material accompanied with OPA. This is indicated in the fourth column as SUB+OPA (M^2 is measured at $P_{in} \sim 5$ W). Now, there are losses both from the material and window. Therefore, the FOM values are low. The effect of PEs is shown in the last two columns, namely for PSF and CGH. For PSF, P_{th} is low, M^2 is high (relatively), and FOM is somewhat high. It is still lower than the empty cavity value though, due to the Fresnel loss mechanism mentioned above. The CGH demonstrates superior values for the parameters of evaluation. It has the lowest M^2 and highest FOM, even when compared to the empty cavity with no loss (note also that M^2 is measured at $P_{in} \sim 6$ W with the CGH).

At this point, a theoretically perfect element can be considered such that Fresnel losses are eliminated by appropriate coatings on the CGH. The discussion that such a perfect coating exists, its applicability, or its performance is not the scope of this paper. Instead, we will speculate on maximum achievable performance via usage of diffractive phase elements. Furthermore, this will guide us in calculating diffractive losses caused by the intra-cavity PEs. The material loss can be estimated by looking at percentage loss. By comparing gray (EMP) and purple (SUB) lines in Figure 4, almost 75% of the power is seen to be gone because of the introduction of the SUB. If this loss is compensated for the CGH, the new FOM becomes approximately 350 μ W and FOM' gets the value of approximately 15×10^{-5} .

For the FOM' values in general, although they follow a similar trend as usual FOM, it is obvious that the CGH-assisted cavity has the highest value from Table 3, almost more than 3 times (from 2.37 for EMP, to 8.89 for CGH). The main factor of using FOM' is to be able to exclude the effect of threshold power, which, essentially, is relatively unimportant with respect to M^2 and slope efficiency, due mainly to operation for higher powers.

Diffractive loss calculations were also made by using simulations. In this case the eigenvalues (γ_{mn}) can be used as indicators of energy conservation, where for a specific modal distribution of Ψ_{mn} , γ_{mn} is between 1 for the lossless case and 0 for total dissipation, as iterations go to infinity. Since the PEs are only intended to generate Gaussian modes, we can specifically use Ψ_{00} and γ_{00} , as modal parameters. The γ_{00} values for our PEs are more than 0.99, both for PSF and CGH. That is in consistent with experimental results, which indicate that the main loss comes from the Fresnel reflections and some absorption coming from materials.

One other point is that the P_{th} is remarkably high in the case of CGH, as seen from the black line in Figure 4. This is reasonable since the CGH is designed for a certain beam size and is not functional for smaller diameters; thus, the laser cannot lase for low powers. This is also a good indicator of the functionality of the CGH design, such that, if we consider low power input, normally the laser is still expected to lase, even in the planar-planar mirror configuration (due to thermal lensing). However, the existence of the CGH modulates the beam the way it is not designed (due to the small beam diameter) and prevents lasing.

Selection of the Gaussian intensity distribution as a desired pattern in CGH design is worth mentioning (see also Section 2.2). The computed CGH surface profile for creating this distribution is shown in Figure 5. The CGH makes little change near the center, where the lowest order beam is strongest, and has more effect in the areas of higher orders. Selection of the desired Gaussian size plays an important role in the design of the CGH. A large diameter Gaussian is formed by a CGH with a large, flat area near the center; increasing the desired Gaussian diameter also reduces the diffraction levels away from the center. At the limit of infinite diameter, the CGH is a flat mirror, since the lowest order mode also has infinite diameter. The majority of the CGH operation is achieved by its central area.

We note that for the intra-cavity elements, especially for the case of a PSF inserted in the cavity, the longitudinal position of the element has little effect on the result. On the other hand, thermal effects, minor alignment issues, and optomechanical and optothermal stability do affect the reliability of results. The assessment of the figures of merit can also be a problem when measurements cannot be taken at the same input-output powers. M^2 measurements couldn't be made at the same input power, especially for a few columns in the table, due to power mismatch, such that for low powers some of the elements cannot be examined, and for high power some elements cause saturation which also hinders measurements. In addition, there are nonlinearities like some thermal lensing at the crystal. We examined thermal lensing, found its focal length as approximately 1.5 m and included that in the calculations. Overall, we can roughly estimate (based on repeated experiments and observations) that our standard deviation should be within 10%.

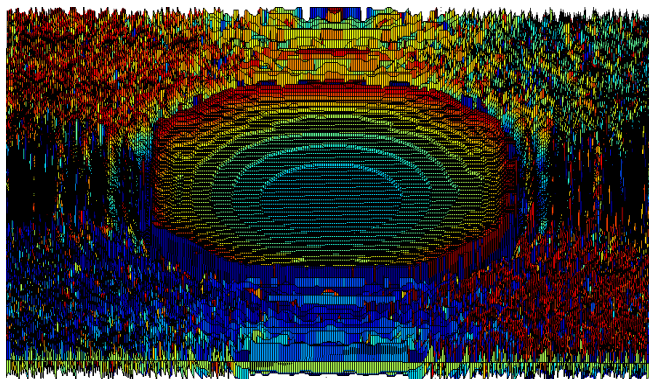


Figure 5. The 4 mm \times 4 mm cross-section (not in scale) of the computed CGH that was used in simulations and experiments.

4. NEW APPLICATIONS

Having examined the fundamental configuration and merits of intra-cavity PEs, we can look at some more innovative applications in this section. Figure 6 indicates some new directions in which the work may evolve in the future. In Figure 6(a), an optically pumped VECSEL setup is seen where a CGH out-coupler is employed. This situation is similar to the work discussed above; there is a certain cavity separation L that designates the resonator. The layout of Figure 6(a) is promising for future VECSEL applications, making it possible to use shorter cavity lengths combined with better performance. The setup is also a transitioning scheme for a more advanced configuration shown in Figure 6(b). Here, a semiconductor laser is shown with a CGH attached to the output. The CGH shapes the mode, i.e., it forces a TEM_{00} mode at higher powers than could be used without the CGH, reducing the beam divergence. Thus, the semiconductor laser will be robust in yielding high-quality beams. The structure can also be envisioned as a compact version of a VECSEL where the elongated resonator length is partly (and implicitly) compensated by the beam shaping capabilities of the CGH.

The configuration in Figure 6(b) suffers from extremely short cavity length. It is necessary to adjust the beam diameter accordingly. Since there is a CGH involved in the laser operation and since the base is a vertical cavity surface emitter, that new form can be named as “holographic cavity surface emitting laser (HOCSEL)”. Although a HOCSEL may have an extremely short cavity length, that length can be extended by adding another material (such as the heat spreader) in the gap, providing (integrated) increased cavity length, still much shorter than a VECSEL, and also providing a method of removing more heat. The physical structure of the HOCSEL unit is similar to that of VCSELs, including distributed Bragg reflectors (DBRs) and quantum wells (QWs). The CGH operates based on Equation (3), where Δn is the index difference between the CGH material and its encapsulating material (it is shown as “gap” below, in Figure 6(b)), rather than between the CGH and the air.

In the integrated version demonstrated in Figure 6(b), the cavity length L , can be defined from the DBR structure to the CGH. The gap, which might also include a few layers inside, is also monolithically integrated to the device. The layers can include a heat spreader and encapsulant of the CGH to facilitate operation, and an extra cavity extension space to increase performance. The main aim here is to decrease that gap as much as possible to ease the integration.

The configurations demonstrated in Figure 6 are being studied and concurrently being developed. Potential issues are related to the laser damage thresholds of PE materials and the effects of the extra small cavity length (which will determine the minimum cavity length). Figure 6 is not intended to be drawn to scale or with a specific size.

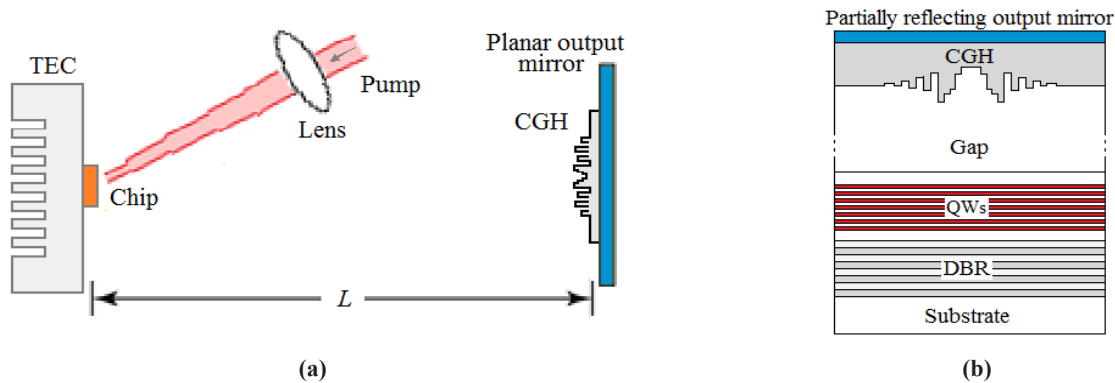


Figure 6. Future potential laser arrangements using intra-cavity PEs. (a) A VECSEL (optically pumped) unit. A CGH is used to modulate the oscillating field in the elongated cavity; this can enable the use of shorter cavity lengths. (b) A HOCSEL unit: a high reflectivity DBR is placed on the laser substrate, followed by QWs grown on top and finished by a gap and a CGH. The partially reflecting output mirror serves as an output coupler. The unit can be pumped electrically or optically through which the CGH side is appropriate to send any pump excitation.

Furthermore, to increase the effect of intra-cavity PEs, a CGH stack can be considered. It was proven in [16] that instead of a single CGH, usage of cascaded CGHs with some buffer layers among them, expands the solution space longitudinally and significantly improves overall performance in 3D imaging. Although the CGH stack was beneficial for 3D image reconstruction as proven, it may, as well, be used for intra-cavity beam shaping to enhance laser performance even further.

5. SUMMARY AND CONCLUSION

As lasers enter widespread use in almost every field, reducing their divergence will imply increasing the quality, which leads to a substantial leap forward in their application. In this work, we proved the feasibility of PEs as a viable option to enhance laser performance in terms of increasing the brightness.

In this work, first, laser cavities were modeled mathematically via usage of the fundamental eigenvalue equation representing round-trip phenomenon of a light field between two resonator mirrors. Different cavity elements were mathematically defined, including different diffractive intra-cavity PEs that were designed and evaluated computationally. Selected PEs, namely a PSF and a CGH, were fabricated and experimentally tested, also accompanied by traditional intra-cavity elements for a systematic and comparative experimental study. By looking at the results, summarized in Section 3.3 and Table 3, diffractive correction is indeed very efficient in decreasing the M^2 value.

Furthermore, energy related FOM values can be increased drastically as well. In summary, even without any AR coating correction, a CGH can diminish M^2 parameter and enlarge brightness more than 3 times approximately. This is a remarkable effect, since this can even be enhanced much more, with material-based preventive measures. To expand this effect, the energy loss mechanism through PEs can be understood more and lessened further. In general, however, it can be said that correction through transparent and diffractive PEs can be much more efficient than using ordinary opaque aperture windows that can cause absorptive loss for beam shaping. At the end, we proposed some new application areas, one of which, introduced as HOCSEL, can be an interesting device to obtain higher powers in single mode semiconductor lasers in a compact and robust manner. Thus, traditional VCSELs can be upgraded with certain trade-offs, which are to be determined in the future work.

The results of improvement in laser performance may have tremendous contributions in the areas of defense, medicine, free-space communications, and range finding. On the other hand, application of diffractive optics to ubiquitous high-power laser resonators can improve laser operation tremendously, yielding a much more convenient way to manipulate beams.

ACKNOWLEDGEMENTS

This work has been supported by the U.S. Air Force Research Laboratory (AFRL), contract number: FA8650-16-C-1761.

REFERENCES

- [1] Siegman, Anthony E. "Laser beams and resonators: beyond the 1960s." *IEEE Journal of selected topics in quantum electronics* 6.6 (2000): 1389-1399.
- [2] H. Kogelnik and T. Li, "Laser Beams and Resonators," *Applied optics* 5, 1550-1567 (1966).
- [3] M. Kuznetsov, Semiconductor disk lasers: Physics and technology, VECSEL semiconductor lasers: A path to high-power, quality beam, and UV to IR wavelength by design (Wiley, 2010).
- [4] D. C. O'Shea, T. J. Suleski, A. D. Kathman, and D. W. Prather, *Diffractive Optics: Design, Fabrication and Test* (SPIE Press, 2004).
- [5] Kol'chenko, A. P., A. G. Nikitenko, and Yu K. Troitskiĭ. "Control of the structure of transverse laser modes by phase-shifting masks." *Soviet Journal of Quantum Electronics* 10.8 (1980): 1013.
- [6] James R. Leger, Diana Chen, and Greg Mowry, "Design and performance of diffractive optics for custom laser resonators," *Applied optics* 34, 2498-2509 (1995).
- [7] Anatolii A. Napartovich, Nikolay N. Elkin, Vera N. Troschieva, Dmitry V. Vysotsky, and James R. Leger, "Simplified intracavity phase plates for increasing laser-mode discrimination," *Applied optics* 38, 3025-3029 (1999).
- [8] Soskind, Y. G., and Igor Anisimov. "Laser cavity mode formation employing diffractive phase structures." In *SPIE Defense+ Security*, pp. 98340G-98340G. International Society for Optics and Photonics, 2016.
- [9] R. Oron, N. Davidson, A.A. Friesem, "Transverse Mode Shaping and Selection in Laser Resonators," *Progress in Optics*, vol. 42.6, pp. 325-386, 2001.
- [10] A.G. Fox and Tingye Li, "Resonant Modes in a Maser Interferometer," *Bell System Technical Journal*, vol. 40.2, pp. 453-488, 1961.
- [11] J. W. Goodman, *Introduction to Fourier Optics*, 3rd ed. (Roberts & Company, 2005).
- [12] David G. Voelz and Michael C. Roggemann, "Digital simulation of scalar optical diffraction: revisiting chirp function sampling criteria and consequences," *Applied optics* 48, 6132-6142 (2009).
- [13] C. C. Davis, *Lasers and Electro-Optics: Fundamentals and Engineering*, 3rd Ed., Cambridge University Press (1996).
- [14] James R. Leger, Diana Chen, and Zhong Wang, "Diffractive optical element for mode shaping of a Nd:YAG laser," *Optics Letters* 19, 108-110 (1994).
- [15] Adam J. Caley, Martin J. Thomson, Jinsong Liu, Andrew J. Waddie, and Mohammad R. Taghizadeh, "Diffractive optical elements for high gain lasers with arbitrary output beam profiles," *Optics Express* 15, 10699-10704 (2007).
- [16] A. Alkan Gülses and B. Keith Jenkins, "Cascaded diffractive optical elements for improved multiplane image reconstruction," *Applied optics* 52, 3608-3616 (2013).